Phase Segregation of Thin Film Polymer Blends on Au Nanopatterned Si Substrates

J. Jerome,* S. Zhu, Y.-S. Seo, M. Ho,† N. Pernodet, R. Gambino, J. Sokolov, and M. H. Rafailovich*

Department of Materials Science and Engineering, State University of New York at Stony Brook, Stony Brook, New York 11794-2275

V. Zaitsev and S. Schwarz

Department of Physics and Astronomy, Queens College, New York 11367

Robert DiNardo

Brookhaven National Laboratory, Uptown, New York 11973

Received December 9, 2003

ABSTRACT: We present a method for producing nano- to submicron scale, chemically heterogeneous surface patterns using an Ar ion mill. To observe the effects of the pattern on dewetting, thin films of PS and PMMA blends were spun-cast and annealed on these surfaces. The results showed that in hole morphologies the as-cast samples phase segregated with $q_2 \sim q_1/2$, where q_2 and q_1 are the wave vectors characterizing the air interface morphology and the Au/Si pattern, respectively. Annealing resulted in the formation of a heterogeneous surface adsorbed phase covered by a PS layer at the air interface. The wave vector of the adsorbed phase, q_4, obeyed the relationship $q_4 \sim q_1/2$ for holes and $q_4 \sim 2q_1$ for islands. The PS layer was observed to completely wet the surface adsorbed layer when the PS and PMMA domains were bicontinuous. Partial wetting occurred when either the PS or PMMA phase in the adsorbed layer was discontinuous.

Introduction

Thin film polymer blends have generated a great deal of interest due to their wide use in a broad range of applications, such as dielectric coatings, lubricants, and lithographic photoresist masks. A primary problem in processing these films is phase separation, which results in delamination and the formation of roughness. Therefore, a large amount of experimental[1−3] and theoretical[4−7] effort has gone into controlling the phase separation process through surface patterning. Most groups have patterned Si wafers with micron-sized chemical gratings. They showed that this method could be used to determine the lateral composition of the film as the two polymers segregate to follow the domains of the underlying pattern. Rockford et al.[8] used a novel method to produce a sinusoidal pattern of Au and Si with a wavelength $\lambda < 50$ nm. In contrast to films placed on the large gratings where only a single length scale is observed, they were able to show that the segregation which occurred in spun-cast polymer films had two length scales. Large-scale, micron-sized phase separation formed on the surface of the film. The structures were unrelated to the surface pattern and were similar to those previously observed on flat Si wafers.[9] When the upper part of the film was removed, a smaller sinusoidal pattern with a period of 60 nm, identical to the underlying pattern, was observed.

In this paper we further explore the case of confinement of a polymer blend film on a chemical pattern with a length scale comparable to the film thickness. Here we focus on the equilibrium configuration and compare both annealed and unannealed films. Using a simple sputtering technique[10] developed in our laboratory, we had previously demonstrated that submicron magnetic Co domains can be patterned on a Si wafer. Here we use the same method to pattern a Si wafer with Au domains of arbitrary size. We then explore the relationship between the dominant wave vector q of the Au/Si pattern and the phase-segregated polymer patterns. We show that by carefully tuning the dominant wave vector of the underlying pattern phase separation of the polymer film can be suppressed.

Suppression of dewetting has also been reported by Fukunage et al.[11] for a polymer blend film spun-cast onto a self-assembled triblock copolymer film grafted onto a Si surface. In this case the relationship between the wave vectors of the surface and blend film patterns was difficult to determine since the dimensions of the pattern were determined by the size of the triblock copolymer, which could not easily be varied.

Experimental Section

Preparation of Patterned Substrates. The patterned surfaces were prepared as follows: A thin layer of Cr (∼80 Å) was first evaporated onto a Si wafer. A second Au layer, 300 Å thick, that was then evaporated on top while still in the vacuum chamber. The samples were exposed to air, and a mixture of monodisperse polystyrene, PS (M_w = 90K), and poly(methyl methacrylate), PMMA (M_w = 27K), was dissolved in toluene and spun-cast directly onto the Au-covered wafers. Since PS and PMMA are immiscible, three-dimensional phase segregation occurred in the spun-cast films. As Stamm et al.[12,13] have shown previously, the morphology of the pattern was controlled by varying the ratio of PS to PMMA in the solution. Here we used mixtures in the weight ratio of 10%, 20%, 30%, 50%, 70%, and 90%. Phase separation was then

* Corresponding authors.
† Present address: Clements High School, Sugar Land, TX 77479.

10.1021/ma030580v CCC: $27.50
Published on Web 07/29/2004

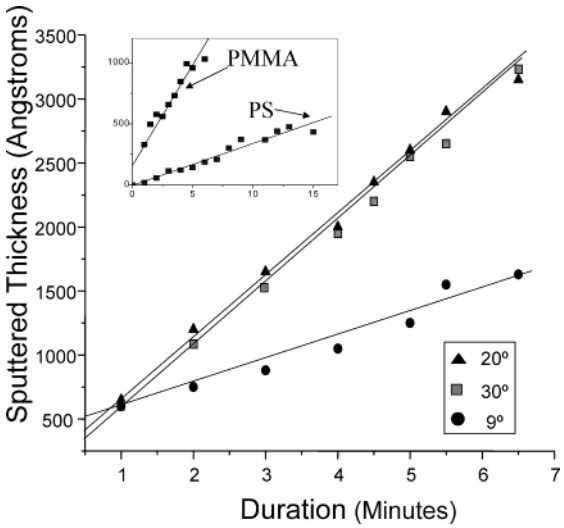

Figure 1. Sputtering rate as a function of time of an Ar ion beam impinging on a 350 nm thick PS film, spun-cast onto a Si wafer. The ordinate axis shows the thickness removed, and the abscissa shows the exposure time to the Ar ion beam. The different traces correspond to different incident angles. Inset: comparison of the thickness vs time for 350 nm PMMA and PS films sputtered at an incident angle of 35°.

allowed to occur by annealing the samples well above their glass transitions ($T_g \sim 100$ and 120 °C for PS and PMMA, respectively) at 180 °C in a vacuum of 10^{-4} Torr for 4 days. The samples were then placed under an Ar ion beam in a Gatan ion mill unit, model 600, with an aperture of 5 mm in diameter.

Surface Etching Conditions. The sputtering conditions were optimized by studying the sputtering rate from uniform films of PS and PMMA spun-cast separately onto Si substrates with a voltage of 2 kV and a current of 0.5 mA. The thickness of the films was measured with a Rudolph three wavelength ellipsometer as a function of sputtering time. The results for PS films are plotted for three different incident angles in Figure 1, where we see that the sputtering rate increases from 170 to 460 Å/min as the incident angle is increased from 9° to 20°. No further improvement occurs when the incident angle is increased to 30° and decreased further to 200 Å/min at an incident angle of 35°. In the inset we compare the thickness as a function of sputtering time for 350 nm PS and PMMA films sputtered at 35°. From the figure we can see that the etching rate of PMMA, 200 Å/min, is significantly faster than that of PS, 70 Å/min.

Secondary Ion Mass Spectrometry and Scanning I Electrom Microscopy. The chemical composition was directly mapped using two techniques: a Leo 1550 scanning I electron microscope (SIEM) and a Cameca ion time-of-flight IV secondary ion mass spectrometer (SIMS). The SIEM was used to obtain an accurate mapping of the final substrate, while the SIMS was used to determine the time evolution of the sputtering.

The Cameca Ion ToF-IV SIMS was equipped with a liquid metal source (Ga) three-lens analyzing gun and a thermal ionization source (Cs) sputtering gun. The incidence angle of the two beams was 45°. The Cs^+ ion beam was rastered over an area of $200 \times 200\ \mu m^2$ in order to sputter layers of a sample. Cs^+ ion energy and current used in this experiment were 3 keV and 40 nA, respectively. The analyzing gun uses isotopically enriched ^{69}Ga with less than 0.1% ^{71}Ga. The analyzing gun was pulsed for 100 ns pulse width and 100 ms cycle time. The Ga^+ ion energy and average current were 25 keV and 1 pA, respectively. The Ga^+ beam was rastered over an area of $20 \times 20\ \mu m^2$ with 256×256 points at the center of the sputtering area of the Cs gun. The sputtering beam was blanked before image acquisition. The charging of the polymer samples was neutralized by using a pulsed low-energy electron flood gun (20 eV, 5 μA current) in between analytical pulses. Negative secondary ion (SI) intensity in the mass range of 1−50 Da was measured for each point of the 256×256 raster. The lateral resolution was better than 0.5 μm. To enhance image contrast, 20 scans were combined. The color scale of the SI intensity was adjusted for each image separately to give best possible representation of the SI images and does not indicate absolute SI intensity.

The results are shown in Figure 2, where we plot the O, C_2H, Au, and Si distribution across the sample surface as a function of sputtering time. From the figure we can see that after 1 min of sputtering we find that the wafer surface is uniformly covered with carbon, and no Au or Si is evident. This indicates that the wafer is fully covered with polymer. From the oxygen trace we find that the droplets do not contain any oxygen, while the substrate is covered with a uniform film of oxygen-rich polymer. We conclude that this layer is PMMA while the droplets are pure PS. After 2 min of sputtering we find a decrease in the PMMA layer and a corresponding increase in the Au distribution. The organic material seems to be concentrated now in the droplets, which also correspond to regions where the Au is not showing. This we interpret as being due to the rapid sputtering of the PMMA layer, which exposes the underlying Au substrate. The droplet sections sputter more slowly, since they seem to be composed only of PS. They screen the Au layer underneath from the sputtering beam. After 3 min of sputtering we find that the Au layer is now sputtered away, revealing the underlying Si substrate. Polymer is still left though in the droplets, and a Au pattern develops on the Si substrate. After an additional 2 min of sputtering, both polymer and Au layers are completely removed, and only a topographical pattern remains imprinted in the Si wafer.

This time sequence is shown graphically in Figure 2b,c where we plot the sputtered intensity of carbon, which corresponds to the organic polymer layer, Au, and Si as a function of sputtering time. In Figure 2b we show the area under the PS droplets, while in Figure 2c we show the area under the PMMA flat regions. From Figure 2c we see that after 1 min of sputtering the PMMA layer is mostly gone and the Au is exposed. On the other hand, in Figure 2b we are still sputtering the PS droplet. After 2 min, Figure 2c shows that we have completely sputtered away the Au regions under the PMMA and have reached the Si layer. On the other hand, in Figure 2b we have just sputtered through the PS layer and began to expose the underlying Au. This sputter time would be the ideal for formation of the Au patterns. If we continue to sputter, then eventually we also eliminate the Au and produce only a topographical pattern on the Si.

The pattern obtained after 3 min of sputtering was also characterized by e-dax elemental mapping and scanning force microscopy. The images are shown in Figure 3. From the figure we find that the sputtered sample has very good fidelity with the original phase-segregated films shown in the left inset. The droplet areas (red, in the topography map) correspond to areas with large carbon content. The blue areas correspond to regions with large Au content. This mapping, performed with higher spatial resolution, is to confirm the TOF-SIMS results.

On the basis of these results, all patterns described in this paper were produced via sputtering the phase-segregated films for 3 min.

Film Preparation for Dewetting Experiments. To observe phase segregation on the patterned surfaces, a 50−50 wt % mixture of PS ($M_w = 90$K) and PMMA ($M_w = 27$K) was dissolved in toluene and spun-cast directly onto the patterned substrates. The film thickness measured by ellipsometry on a flat Si substrate was about 600 Å. The samples were then annealed for 7 days at 170 °C in a vacuum of 10^{-4} Torr. On the basis of previous studies of the time evolution of the pattern,[9] the annealing time was selected so as to ensure equilibrium conditions were achieved. The chemical composition of the film was obtained by rinsing in cyclohexane at 28−30 °C. At this temperature cyclohexane is a differential solvent which dissolves only the PS phase. The PMMA phase was determined by rinsing in acetic acid, which is a differential

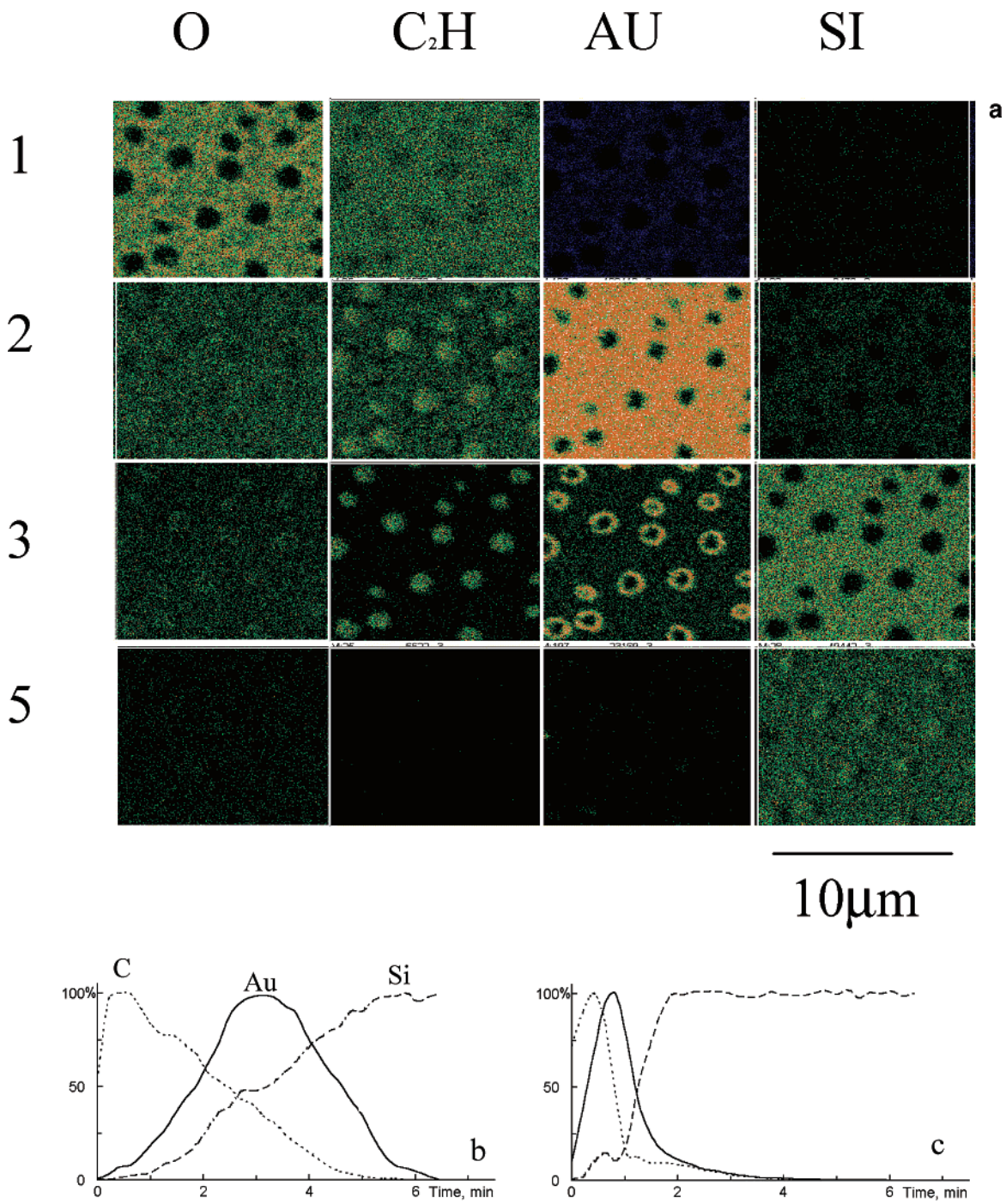

Figure 2. (a) O, C_2H, Au, and Si distributions across the sample surface are plotted as a function of sputtering time. After 1 min of sputtering, the wafer is fully covered with polymer. After 2 min of sputtering, we find a decrease in the PMMA layer and a corresponding increase in the Au distribution. After 3 min of sputtering, the Au layer is now sputtered away, revealing the underlying Si substrate. After 5 min of sputtering, both polymer and Au layers are completely removed. (b) The normalized sputtering intensity plotted as a function of time for C, Au, and Si traces when the beam is positioned on the dewetted (PS) droplet. (c) The normalized sputtering intensity plotted as a function of time for C, Au, and Si traces when the beam is positioned on the flat PMMA region.

solvent only for the more polar PMMA. It was not possible to analyze these films and thereby identify the phases using scanning transmission X-ray or electron microscopy since the Au films were invariably removed with the polymer layers when the samples were floated onto grids.

Results and Discussion

The patterned surfaces are shown in column 1 of Figure 4, corresponding to the original blend compositions of weight ratio of 10%, 20%, 30%, 50%, 70%, and 90% PS to PMMA. The patterns are composed of either hole or island morphologies, except in pattern 1F, which is a combination of large holes and small islands. The patterns are characterized by two parameters: D, the average hole or island diameter, and L, the center-to-center distance. These values were measured from the AFM images using Photoshop and averaging over at least 20 holes or islands. These values are listed in Table 1. Fast Fourier transforms (FFT) were also performed

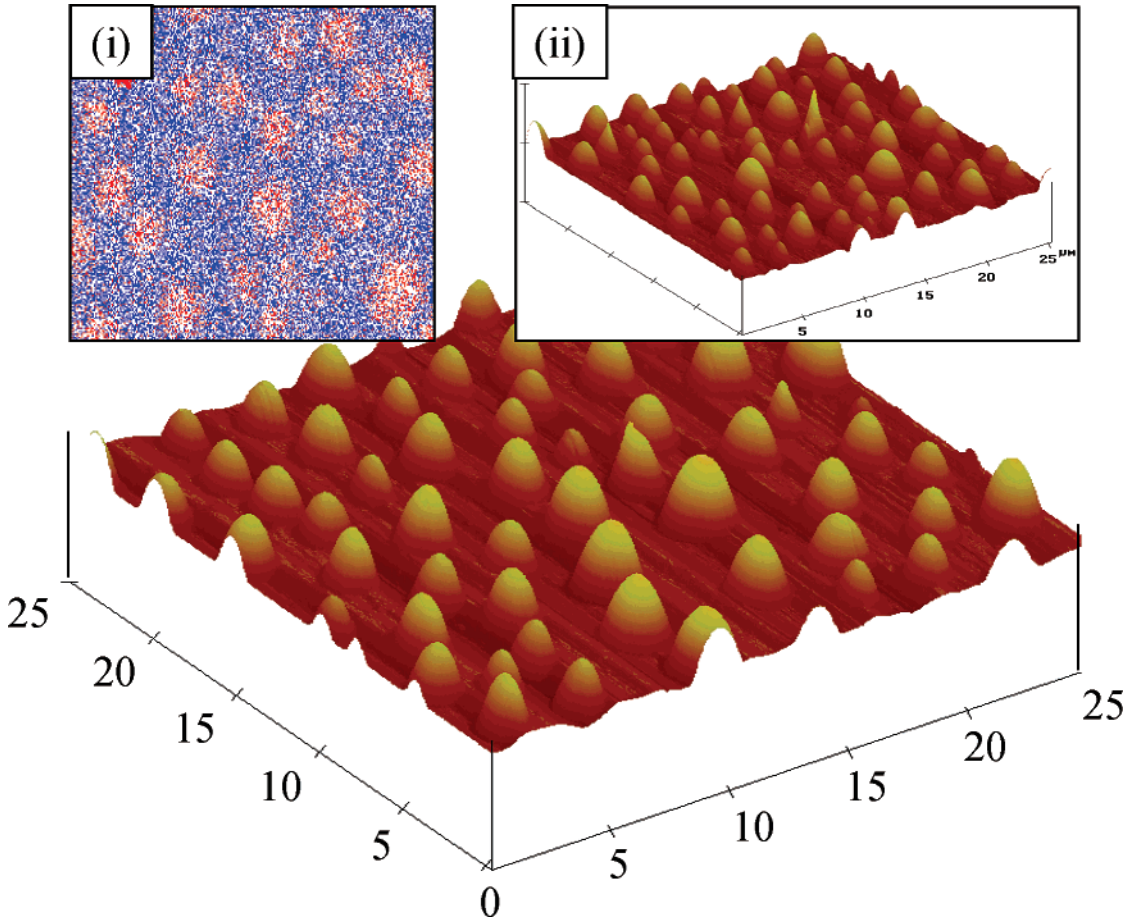

Figure 3. Pattern obtained after 6 min of sputtering was characterized by e-dax elemental mapping (inset i) and scanning force microscopy (inset ii) and is superimposed on the scanning force microscopy image before sputtering. The droplet areas (red, in the topography map) correspond to areas with large carbon content. The blue areas correspond to regions with large Au content.

on some of the images, and the results are shown as insets in Figure 4. The dominant wave vectors, q, for each surface obtained from the ring shown in the insets are tabulated in Table 2. From Tables 1 and 2 we determined the center-to-center distance according to $L = 2\pi/q$.

The height of the islands or depth of the holes was slightly smaller than the thickness of the initial Au layer or 25 nm.

The morphologies of the as-cast films on the surfaces are shown in column 2. Here we see that the film is uniform on the pattern with the smallest hole diameter (2A). A larger degree of phase segregation is observed on patterns 2B and 2C, where the hole diameter, D, has increased. From the image and the FFT analysis we see that the wave vector of the phase-segregated patterns on 2B and 2C are similar, even though from Table 2 we find that the hole diameter, D, increases by a factor of 2.7. On the other hand, the center-to-center distance, L, or the dominant wave vector, q_{2B} and q_{2C}, is unchanged. Hence, we conclude that for the as-cast film the q vector or L, rather than the size of the surface Au pattern, D, determines the phase-segregated structure. Furthermore, from Table 2 we see that the wave vector of the surface chemical pattern, q_1, is related to the wave vector of the phase-segregated morphology, q_2, according to $q_1 \approx 2q_2$, in hole morphologies B and C.

The case of the phase-segregated morphology on the island structures is somewhat more complicated, and no clear correlation with any specific length scale of the surface pattern in 2D and 2E could be made. The mixed morphology in 2F shows two values for q_2, where the smaller one is similar to q_{1F}. Since the as-cast films are nonequilibriated and the morphology depends on the spin-casting conditions, it is difficult to interpret these structures in further detail.

In column 3 we show the surface morphology after annealing the film shown in column 2. Here we observe that the morphologies of 3A, 3B, and 3E are now similar. The patterns show droplets, which only partially wet a substrate layer. The contact angles, obtained by averaging over four to five droplets on the substrate layer using AFM,[14] are tabulated in Table 2, where we see that they decrease monotonically from 3A to 3E. The films on surfaces C, D, and F are now topographically flat, even though the underlying patterns are very different, i.e., hole, island, or mixed structures. From Table 2 we see that the chemical patterns on these surfaces all have different q_1 vectors. On the other hand, from Table 1 we find that patterns C and D have similar average diameters of the island or hole features. We can further postulate that as the value of D increases, the contact angle of the dewetted droplets decreases. When a value of $D \sim 3200$ Å is reached, complete wetting occurs in both islands and holes morphologies. As D increases further (pattern 3E), phase segregation is resumed as the domain size approaches the scale of the droplets. In pattern F, the smaller value of D is similar to that for pattern B while the larger value is similar to that of E. Even though the film dewets both of these surfaces, it is interesting to note that when both length scales are combined dewetting is suppressed again. Hence, in

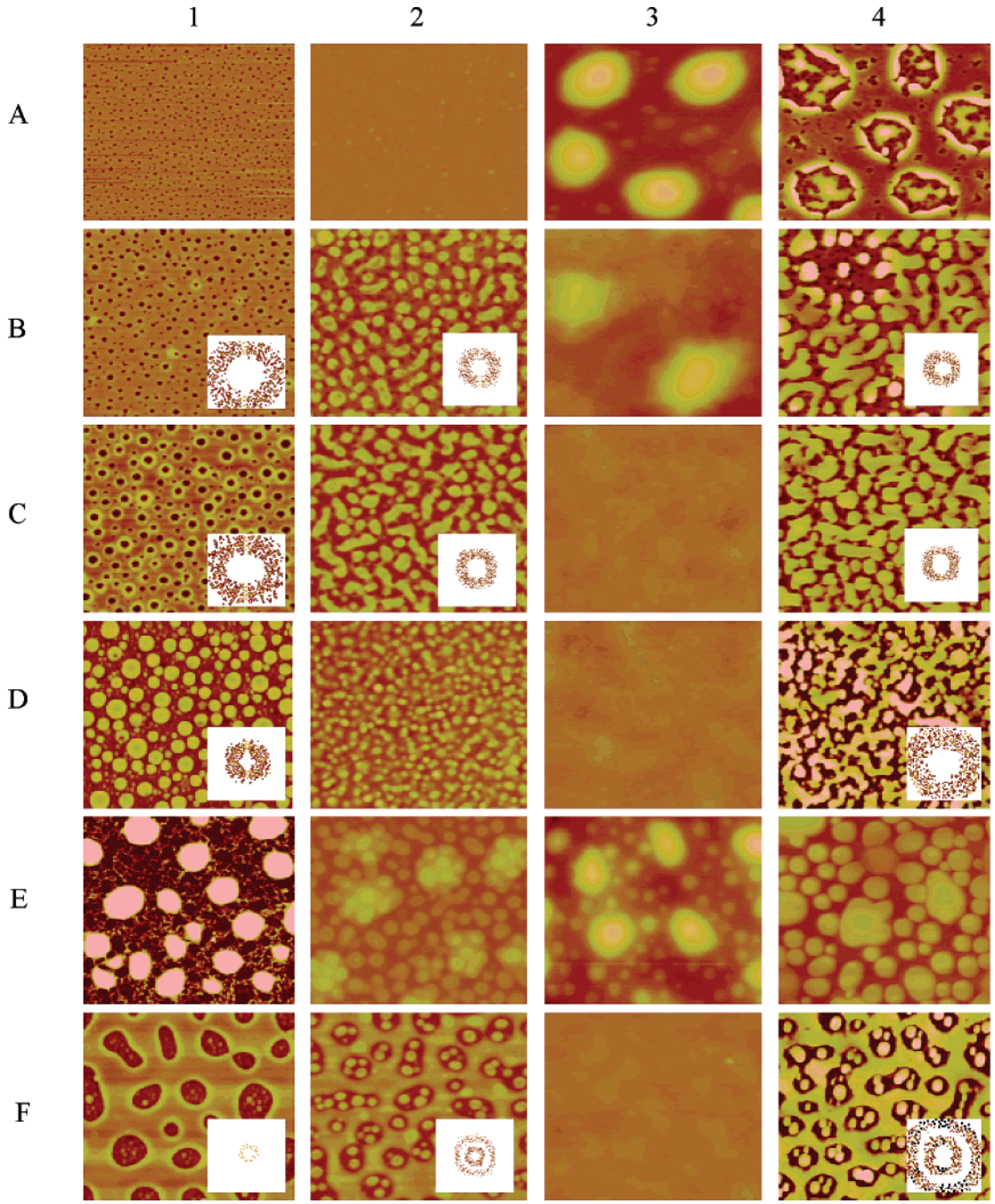

Figure 4. Column 1 (A−F): Pattern of Au on Si made by the Ar ion etching method described in the Experimental Section. In A−C the holes are Si while the uniform area is Au. In D and E, the islands are Au and the uniform region is Si. F is a mixed hole/island configuration where the uniform region outside holes is Au and inside holes is silicon. Column 2 (A−F): AFM topography scan of as-cast PS/PMMA on the pattern in column 1. Inset: fast Fourier transform of the images. Column 3 (A−F): AFM topography scan of the films in column 2 after annealing 7 days at 170 °C in a vacuum of 10^{-4} Torr. Column 4 (A−F): AFM topography scan of the annealed film after immersion in cyclohexane for 40 min to remove the PS phase. Inset: fast Fourier transformation of images.

the annealed film it appears that D rather than q of the underlying patterns determines whether the polymer film completely or partially wets the adsorbed polymer layer on the substrate.

To map the lateral chemical composition of the film, the PS phase was removed by soaking in cyclohexane for 40 min. The surface morphology, after washing, is shown in column 4, where the remaining structures are composed only of PMMA. On surface 4A we find that the large round droplets were removed, which leads us to conclude that they were mainly PS. The polymer remaining in the flat areas must therefore be mainly PMMA. This phase-segregated morphology where only PMMA is continuous similar to that previously reported on flat Si.[9] It is interesting to note at this point that PMMA clearly prefers the Au covered substrate. This is in contrast to the results reported by Rockford et al.[8] where a slight preference for the Au was observed for their PS polymer. Since, as Rockford shows, neither PS nor PMMA interacts strongly with Au, slight differences in surface preparation or in tacticity of the specific polymers used may affect these results.

Except in 4A and 4E, we find an adsorbed phase, which is not correlated to the morphology at the film

Table 1. Characterization of Au/Si Pattern

pattern	structure	av size D (nm)	separation L (nm)	contact angle of polymer droplet (deg)
A	hole	70	185	12.3
B	hole	110	320	7.5
C	hole	320	310	*a*
D	island	370	620	*a*
E	island	900	1000	4.6
F	hole	820	1250	*a*
	island	110	80	

[a] Complete wetting.

Table 2. Wave Vectors Characterizing the Surface and Polymer Patterns

	Q vector of pattern substrate (nm^{-1}) q^1	Q vector of as-cast film (nm^{-1}) q^2	Q vector of PMMA (nm^{-1}) q^4
B	0.02	0.012	0.01
C	0.020	0.013	0.011
D	0.01		0.022
F	0.005	0.015	0.03
		0.007	0.013

surface shown in column 3. Here the PMMA is seen to form a pattern with well-defined wave vectors in both flat and droplet morphologies. For hole patterns, B and C, we find that the wave vector of the PMMA is approximately equal to that of the as-cast pattern and half of the value of the underlying chemical patterns, i.e., $q_4 \sim q_2 \approx q_1/2$. In contrast on the island morphology, 1D, we find $q_4 \sim 2q_1$ of the Au/Si pattern, which is similar to the results of ref 3.

For the mixed morphology (4F) the PMMA structure has two well-defined wave vectors where each one is roughly twice the corresponding value in the as-cast film shown in 2F. Hence, this structure is similar to the "island" category.

The total thickness of all the film was measured before washing using ellipsometry and found to be approximately 600 Å. The height of the PMMA structures shown in Figure 4B−F was measured by cross-sectional analysis of the AFM images and found to be approximately 400 Å.

We can then interpret the results as follows: PMMA is preferentially adhered to the Au interface while PS is preferred at the vacuum surface. The preferential adhesion of PMMA to Au is already observed in the as-cast samples (column 2). Upon annealing at 170 °C the PS and PMMA segregate to the vacuum surface and Au interfaces, respectively. The ability of the PMMA to conform to the Au pattern seems to depend on the size and curvature of the features. Qualitatively, the equilibrium conformation of the PMMA is a balance between the gain in enthalpy achieved by forming PMMA/Au contacts and the unfavorable bending energy required to follow features with steep curvature. Hence, the PMMA does not conform to the small hole pattern in 1A where a large degree of bending is required. As the diameter of the holes increases, the PMMA is seen to form an interconnected structure, which allows it to follow the Au pattern while minimizing curvature. This results in the formation of the surface adsorbed phase where the PS and PMMA region become increasingly bicontinuous. The structure of this phase affects the behavior of the PS layer at the air interface. On pattern 4A, where the PMMA is unaffected by the holes, the contact angle is 12.3°, which is similar to that previously reported[15] on a flat Si surface. As the underlying layer becomes increasingly heterogeneous, the contact angle with PS decreases. From Figure 4 we see that when the patterns are completely bicontinuous (C, D), complete wetting occurs. When either the PS phase or the PMMA phases are discontinuous (surface A and E), dewetting of the substrate occurs. In the case of surface B, we note that the PMMA phase is bicontinuous only in a small section of the sample; hence, the contact angle is decreased but not totally eliminated. The mixed morphology does not fit this pattern, and we do not quite understand it as yet.

To confirm that these features are due only to the chemical heterogeneity rather than the topographic features, patterns were also etched onto pure Si wafers with native oxide layer. The height of the Si structures was approximately 50 nm, which was comparable to

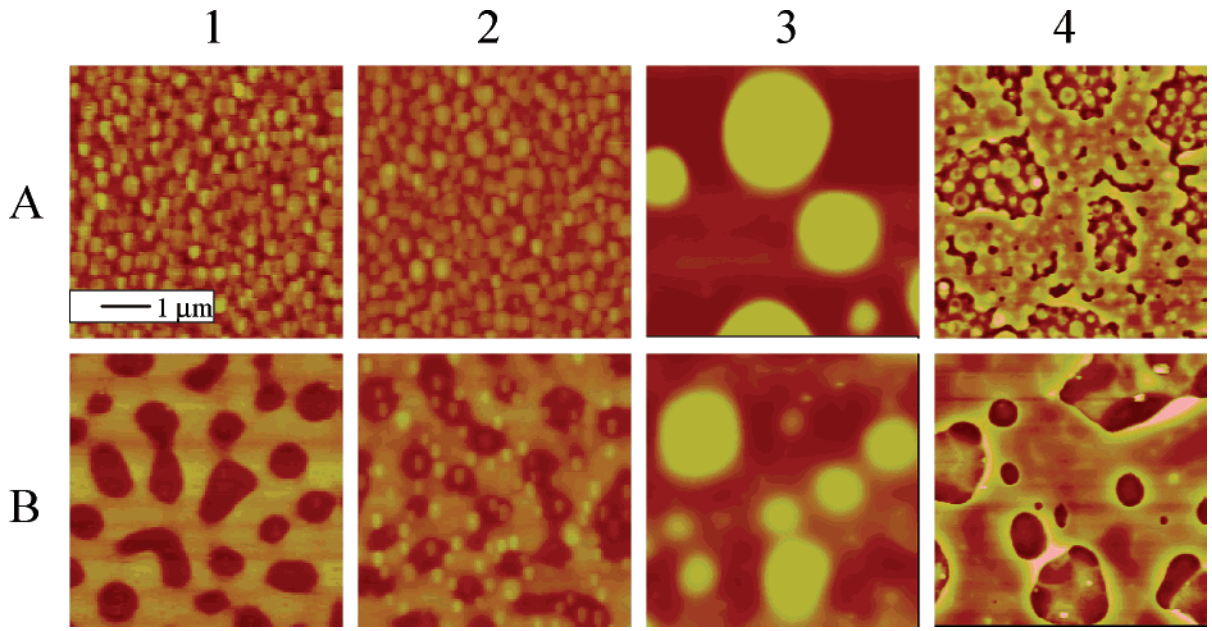

Figure 5. Column 1: Two patterns etched into a native oxide-covered Si wafer. Note the resulting patterns are similar to D and F of Figure 4 in size D and separation L. Column 2: Morphology of the as-spun PS/PMMA film. Column 3: Morphology of the film after annealing 7 days at 170 °C in a vacuum of 10^{-4} Torr. Column 4: Morphology after washing in cyclohexane for 40 min.

that of the Au features since the same masks were used. The topography of two typical samples with island and hole patterns, A and B, respectively, are shown in column 1 of Figure 5. From the figure we see that the features have wave vectors comparable to surfaces D and F. In column 2 we show the morphology of the as-cast film, where we see that it resembles the underlying pattern. The surface morphology after annealing (with the same conditions as in Figure 4) is shown in column 3. Here we see that large droplets are formed which dewet the underlying film with $\theta = 12.2°$, which is similar to the value measured for 3A and reported[14] for the flat surface. The morphology of the samples dipped in cyclohexane is shown in column 4. Here we see that, as before, the droplets are PS while the continuous phase is PMMA. No heterogeneous surface adsorbed phase is present. The PMMA completely wets the Si regardless of the topography of the sublayer. Hence, at equilibrium the morphology of the blend film is to first-order independent of the underlying pattern. From these results we conclude that the chemical heterogeneity of Au/Si pattern rather than the topographical roughness is responsible for the structures observed in Figure 4.

Conclusion

In conclusion, we have shown the chemically heterogeneous surface can be patterned by Ar ion milling through a polymer mask. The patterns were characterized by the diameter of the patterns, D, and the wave vectors, q. To observe the effects of the pattern on dewetting, thin film of PS and PMMA blends were spun-cast and annealed on these surfaces. The results showed that in hole morphologies the as-cast samples phase-segregated with $q_2 \sim q/2$. Annealing resulted in the formation of a heterogeneous surface adsorbed phase covered by a uniform PS layer at the air interface. The wave vector of the adsorbed phase was $q_4 \sim q_1/2$ for holes and $q_4 \sim 2q_1$ for islands. The PS layer was observed to completely wet the surface adsorbed layer when the PS and PMMA domains were bicontinuous.

Acknowledgment. This work was supported by the NSF-MRSEC program (DMR 9632525). M. Ho acknowledges support from AT&T, the Keyspan Corp., and SUNY AGEP for their support for the last three years.

References and Notes

(1) Boltau, M.; Walheim, S.; Mlynek, J.; Krausch, G.; Steiner, U. *Nature (London)* **1998,** *391*, 877. Krausch, G.; Kramer, E. J.; Rafailovich, M.; Sokolov, J. *Appl. Phy. Lett.* **1994,** *64*, 2655.
(2) Karim, A.; Douglas, J. F.; Lee, B. P.; Glotzer, S. C.; Rogers, J. A.; Jackman, R. J.; Amis, E. J.; Whitesides, G. M. *Phy. Rev. E* **1998**, *57*, R6273. Chaudhury, M.; Whitesides, G. M. *Science* **1992**, *256*, 1539.
(3) Nisato, G.; Ermi, B. D.; Douglas, J. F.; Karim, A. *Macromolecules* **1999**, *32*, 2356.
(4) Gleiche, M.; Chi, L. F.; Fuchs, H. *Nature (London)* **2000**, *403*, 173.
(5) Kataoka, D. E.; Troian, M. S. *Nature (London)* **1999**, *402*, 794.
(6) Gau, H.; Herminghaus, S.; Lenz, P.; Lipowsky, R. *Science* **1994**, *263*, 60.
(7) Kargupta, K.; Sharma, A. *Phy. Rev. Lett.* **2001**, *86*, 4536.
(8) Rockford, L.; Liu, Y.; Mansky, P.; Russell, T. P.; Yoon, M.; Mochrie, S. G. J. *Phys. Rev. Lett.* **1999**, *82*, 2602−05.
(9) Ade, H.; Winesett, D. A.; Smith, A. P.; Qu, S.; Ge, S.; Sokolov, J.; Rafailovich, M. *Europhys. Lett.* **1999**, *45*, 526.
(10) Zhu, S.; Gambino, R. J.; Rafailovich, M. H.; Sokolov, J.; Schwarz, S. A.; Gomez, R. D. *IEEE Trans. Magn.* **1997**, *33*, 3022−3024.
(11) Fukunaga, K.; Elbs, H.; Krausch, G. *Langmuir* **2000**, *16*, 3474.
(12) Gutmann, J. S.; Müller-buschbaum, P.; Schubert, D. W.; Stribeck, N.; Stamm, M. *J. Macromol. Sci., Phys.* **1999**, *B38*, 563.
(13) Affrossman, S.; Henn, G.; O'Neill, S.; Pethrick, R.; Stamm, M. *Macromolecules* **1996**, *29*, 5010.
(14) Israels, R.; Jasnow, D.; Balazs, A. C.; Guo, L. Krausch, G.; Sokolov, J.; Rafailovich, M. H. *J. Chem. Phys.* **1995**, *102*, 8149.
(15) Qu, S.; Clarke, C. J.; Liu, Y.; Sokolov, J.; Rafailovich, M. *Macromolecules* **1997**, *30*, 3640.

MA030580V